





Article

Preparation, Features, and Efficiency of Nanocomposite Fertilisers Based on Glaucanite and Ammonium Dihydrogen Phosphate

Maxim Rudmin ^{1,2,*} , Boris Makarov ¹, Adrián López-Quirós ³ , Prokopiý Maximov ¹ , Valeria Lokteva ¹ , Kanipa Ibraeva ², Alexander Kurovsky ⁴, Yana Gummer ⁴ and Alexey Ruban ¹

¹ School of Earth Science & Engineering, Tomsk Polytechnic University, 634050 Tomsk, Russia; makar189@mail.ru (B.M.); pnm1@tpu.ru (P.M.); ruban@tpu.ru (A.R.)

² Institute of Environmental and Agricultural Biology (X-BIO), University of Tyumen, 625003 Tyumen, Russia

³ Department of Stratigraphy and Paleontology, University of Granada, 18071 Granada, Spain

⁴ Department of Plant Physiology and Biotechnology, Biological Institute, Tomsk State University, 634050 Tomsk, Russia; a.kurovskii@yandex.ru (A.K.)

* Correspondence: rudminma@tpu.ru or rudminma@gmail.com; Tel.: +7-8-3822-60-62-45

Abstract: This paper studies the chemical and mechanochemical preparation of glauconite with ammonium dihydrogen phosphate (ADP) nanocomposites with a ratio of 9:1 in the vol.% and wt.%, respectively. The methods include X-ray diffraction analysis, scanning electron microscope with energy-dispersive X-ray spectroscopy, transmission electron microscopy, infrared spectroscopy, and differential thermal analysis with a quadruple mass spectrometer. The manufactured nanocomposites keep the flaky glauconite structure. Some glauconite unit structures have been thickened due to minimal nitrogen (ammonium) intercalation into the interlayer space. The globular, granular, or pellet mineral particles of nanocomposites can be preserved via chemical techniques. Globular and micro-aggregate particles in nanocomposites comprise a thin film of adsorbed ADP. The two-step mechanochemical method makes it possible to slightly increase the proportion of adsorbed (up to 3.2%) and intercalated (up to 6.0%) nutrients versus chemical ways. Nanocomposites prepared via chemical methods consist of glauconite (90%), adsorbed (1.8–3.6%), and intercalated (3.0–3.7%) substances of ADP. Through the use of a potassium-containing clay mineral as an inhibitor, nitrogen, phosphorus, and potassium (NPK), nanocomposite fertilisers of controlled action were obtained. Targeted and controlled release of nutrients such as phosphate, ammonium, and potassium are expected due to various forms of nutrients on the surface, in the micropores, and in the interlayer space of glauconite. This is confirmed via the stepwise dynamics of the release of ammonium, nitrate, potassium, and phosphate from their created nanocomposites. These features of nanocomposites contribute to the stimulation of plant growth and development when fertilisers are applied to the soil.

Keywords: glauconite; ammonium dihydrogen phosphate; controlled-release fertiliser; potassium; chemical activation; mechanochemical activation



Citation: Rudmin, M.; Makarov, B.; López-Quirós, A.; Maximov, P.; Lokteva, V.; Ibraeva, K.; Kurovsky, A.; Gummer, Y.; Ruban, A. Preparation, Features, and Efficiency of Nanocomposite Fertilisers Based on Glaucanite and Ammonium Dihydrogen Phosphate. *Materials* **2023**, *16*, 6080. <https://doi.org/10.3390/ma16186080>

Academic Editor: Yeong-Joon Park

Received: 19 August 2023

Revised: 3 September 2023

Accepted: 4 September 2023

Published: 5 September 2023



Copyright: © 2023 by the authors. Licensee MDPI, Basel, Switzerland. This article is an open access article distributed under the terms and conditions of the Creative Commons Attribution (CC BY) license (<https://creativecommons.org/licenses/by/4.0/>).

1. Introduction

Today, sustainable agriculture is crucial to providing the growing global population with sufficient food [1–4]. To achieve this goal, developing new types of fertilisers and technologies for their use aims to improve the efficiency of modern and future agriculture [5–7]. However, using traditional fertilisers such as urea or carbamide, due to their high solubility and low thermal stability, are capable of causing a short-term increase in agricultural production, while their uncontrolled use leads to risks of environmental damage [8–11]. A representative example is the analysis of the environmental state in areas of developed agriculture, where greenhouse effects [12], eutrophication of water bodies [13], and other negative consequences of the use of traditional nitrogen fertilisers have been identified.

Due to the limited phosphate mineral base, phosphate fertilisers are used less than nitrogen fertilisers [14,15]. On the other hand, sometimes, the production of phosphorus fertilisers from phosphate rocks leads to the pollution of the environment by radioactive by-products and heavy metals [16]. In addition, many mineral phosphate fertilisers exist in unavailable forms [17]. Therefore, using mineral phosphate fertilisers can lead to inefficient use of available phosphates by plants. For improved plant nutrition, synthetic phosphate substances such as ammonium phosphates are applied [18]. The long-term effect of ammonium phosphate is achieved via its encapsulation in the membranes of various substances [19–24]. Among the new types of fertilisers are slow-release or controlled-release fertilisers [7,25–30].

Controlled-release fertilisers (CRF) are usually complex materials consisting of substances with separated functions [5,25,31]. The key components of CRF are nutrients (often ammonium or phosphates) and inhibitory substances [27,32,33]. Various polymers [25,34–37], organic materials [22,28,38–40], minerals [41–46], and heterogeneous substances [44,47–51] can inhibit nutrients in the CRF. Clay minerals (phyllosilicates) are common inorganic materials in the creation slow-release fertilisers [41,45,52–62]. Clay minerals and clay-based complex materials are also used to purify water from phosphate and ammonium ions [63,64]. Phyllosilicates such as vermiculite, montmorillonite, kaolinite, halloysite, and sepiolite are considered relatively inexpensive and environmentally friendly adsorbents of different ions from polluted waters [65]. Glauconite is a potassium-containing dioctahedral phyllosilicate [66,67] that has recently been examined as a urea inhibitor in CRF [43,57]. At the same time, glauconite and glauconite rocks improve soil fertility and plant growth [46,68–74], making it possible to evaluate them as promising composite materials in the creation of modern multifunctional fertilisers.

The research aimed to prepare glauconite–phosphate nanocomposites using the methods of chemical and mechanochemical activation, with an assessment of the relationship between the mineral as a multifunctional inhibitor and ammonium dihydrogen phosphate as a nutrient.

2. Materials and Methods

2.1. Materials

This research used a glauconite sample (Karin deposit, Russia) as an inhibitor. The glauconite sample is composed of 70 wt.% glauconite and a 30 wt.% mixture of quartz and feldspars. The average chemical composition of glauconite is as follows [75]: 44.6–56.5 wt.% SiO₂; 3.5–11.4 wt.% Al₂O₃; 17.5–29.8 wt.% Fe₂O₃(total); 6.5–8.8 wt.% K₂O; 2.6–4.5 wt.% MgO; m0.6–0.8 wt.% CaO; 0.3–0.4 wt.% Na₂O; and 1.7–14.5 wt.% loss on ignition (LOI). The typical formula of glauconite, measured via energy dispersive analysis, is as follows: K_{0.6–0.8}(Al_{0–0.8}Mg_{0.3–0.5}Fe_{0.9–1.5})_{1.4–2.3}(Si_{2.9–4.0}Al_{0.0–0.5})O₁₀(OH)₂nH₂O.

XRD patterns of the air-dried clay fraction and ethylene glycol saturation of the initial glauconite sample (Figure 1) display around 5–8% of an expanded smectite phase based on the shift 001 basal peaks from ~12.6 Å to ~18.6 Å [75].

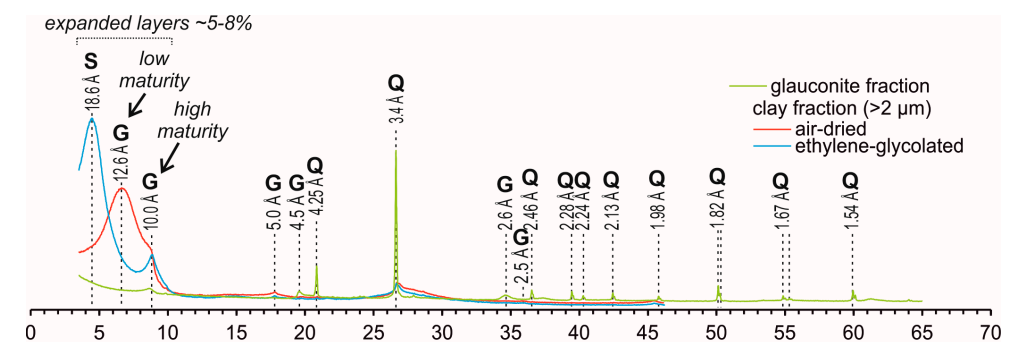


Figure 1. X-ray diffraction patterns of initial glauconite fraction and its oriented clay fractions. G—glauconite; S—smectite; Q—quartz.

2.2. Preparation of Nanocomposites

Ammonium dihydrogen phosphate (ADP; $\text{NH}_4\text{H}_2\text{PO}_4$) was used as a filling nutrient. ADP consists of more than 15% P_2O_5 and 4% nitrogen. The process for creating nanocomposites using glauconite and ADP was executed through four distinct methods: (1) a one-step chemical method; (2) a two-step chemical method with the sodium carbonate; (3) a two-step mechanochemical method of ring milling; and (4) a two-step mechanochemical method of planetary milling. The one-step chemical method involves impregnating the globular glauconite fraction (90 g) in the ADP solution–gel (10 mL) for 48 h until a dry state is reached. The two-step chemical method includes the preliminary impregnating of the globular glauconite fraction (90 g) by the extender (Na_2CO_3) and the subsequent activating of the ADP solution–gel (10 mL) for 48 h. The final nanocomposites prepared via the one-step and two-step chemical methods were called Gko90P10 and GkNa90P10, respectively. Mechanochemical activation is distinguished from chemical activation in that it involves grinding glauconite in various mills without employing solutions in the initial stage. The mechanochemical method was subdivided into two variants. Each variant was composed of two steps. The first step is activating the glauconite fraction via ring or planetary milling. The ring milling operation was conducted by a ROCKLABS Standard Ring Mill (with a rotation frequency of 700 rpm and a mass ratio of powders to grinding bodies of 1:5) for 10 min. The planetary milling operation was carried out by AGO-2 with a 1:5 ratio of powder to grinding bodies and a rotation frequency of 1820 rpm for 1 min. The second step is soaking the activated glauconite fraction (90 g) in the ADP solution–gel (10 mL) for 48 h until a dry state is reached. The final nanocomposites produced via two-step mechanochemical methods of ring or planetary milling were named Gka90P10rm and Gka90P10pm, respectively.

2.3. Nanocomposite Analysis

The fabricated nanocomposites underwent a series of analyses using X-ray diffraction analysis (XRD), scanning electron microscopy with energy dispersive X-ray spectroscopy (SEM–EDS), transmission electron microscopy (TEM) with selected area electron diffraction (SAED), Fourier transform infrared spectroscopy (FTIR), and differential thermal analysis (thermogravimetric analysis and differential scanning calorimetry, TG–DSC) paired with a quadruple mass spectrometer (MS).

Before and after the nanocomposites' activation, glauconite structural changes were evaluated. The crystal composition of nanocomposites was identified using a Bruker D2 Phase X-ray diffractometer (Billerica, MA, USA). It used Cu $\text{K}\alpha$ radiation with a voltage of 30 kV and a current setting of 10 mA. Separated fractions with less than 10 μm in size were scanned from 4° to 70° 2-Theta at a step increment of 0.02° with a scan pace of 1.5 s/step. Furthermore, the clay portion with less than 2 μm in size from all nanocomposites, as well as the initial one, was separated then suspended in distilled water, settled for 8–16 h, and then air dried on glass panels. Each sample was assessed in the air-dried and ethylene glycol-solvated states after 24 h in a desiccator at roughly 60°C . Methods described in [76,77] were used to identify glauconite and smectite. Quantitative mineral evaluation was accomplished using Rietveld analysis [78] with PDXL and Siroquant software packages [79].

The nanocomposites were investigated using the TESCAN VEGA 3 SBU scanning electron microscope (Brno, Czech Republic) and an OXFORD X-Max 50 energy-dispersive adapter (High Wycombe, UK). The SEM–EDS scanning was conducted at a specimen current of 3–12 nA, a spot diameter of $\sim 2 \mu\text{m}$, and an accelerating voltage of 20 kV.

The JEOL JEM-2100F transmission electron microscopy (TEM, Tokyo, Japan) at the Center for Sharing Use “Nanomaterials and Nanotechnologies” of Tomsk Polytechnic University was employed to observe crystal structure of glauconite. Specimens were prepared by drying a nanocomposite droplet on a carbon-film-coated copper grid. The TEM analysis was carried out at 200 kV.

The FTIR spectrometer (Shimadzu FTIR 8400S, Kyoto, Japan) chartered the spectra of the nanocomposites between 4000 and 400 cm^{-1} with KBr pellets, a resolution of 4 cm^{-1} . This was conducted to ascertain the nanocomposites' chemical bond functional groups.

Using a STA 449 F5 Jupiter (NETZSCH, Selb, Germany) micro-thermal analyser, the TG–DSC curves were plotted across temperatures ranging from 30 to 1000 $^{\circ}\text{C}$ in an argon setting with a heating rate of 10 $^{\circ}\text{C}/\text{min}$. This facilitated the quantification of the weight ratio of different forms of adsorbed and intercalated substances and a study into thermal degradation. The TG–DSC–MS analysis was realised using a Netzsch TA Quadrupole Mass Spectrometer (QMS) 403C Aeolos for quantification and identification of the evolved gases. Calibration was undertaken just before testing, and the mass spectrometer functioned in electron impact ionisation mode, monitoring ions for the mass-to-charge (m/z) ratios from 1 to 50.

2.4. Leach Testing

Surface soil was collected from agricultural lands in the Tomsk region of Western Siberia (Russia). After root extraction and room temperature drying, the soil was sieved to under 2 mm. A total of 80 g of this dried soil was combined with either nanocomposite in a PVC tube at a dose equivalent to 380 $\text{mg N}\cdot\text{kg}^{-1}$. Specific quartz sand quantities were added atop each soil column, and the experiment involved three replications per tested item (three replicates of each sample were called a “plot”).

Soil moisture was retained at 75%. On days 1, 4, 7, 14, 21, 28, 42, and 56, each soil column received 200 mL of deionised water, and the resultant leached solutions (the filtrates) were collected for analysis. The pH, potassium (K^+), ammonium (NH_4^+), and nitrate (NO_3^-) concentrations of filtrates were determined using the ionometric method, and phosphate (P_2O_5) concentrations were measured using spectrophotometric techniques. Resultant plot values were calculated as the average of three replicates. The cumulative release curves of potassium (K^+), ammonium (NH_4^+), nitrate (NO_3^-), and phosphate (P_2O_5) were calculated for interpretation.

2.5. Plant Cultivation Test

In-lab growth experiments for agricultural plants were performed via the addition of nanocomposites. Soil without fertilisers was used as a control and rationing plot. Weakly acidic agricultural soil (pH 5.1) with 4% organic carbon was used for the tests. Oat seeds (*Avena sativa*) were cultivated under room conditions for 20 days. Dry nanocomposites were introduced to the soil at 50 kg (potassium) per ha. All tests were conducted thrice (one plot). Germination was estimated after 4 days as the ratio of sprouts to the number of seeds sown. After 20 days, measurements for plant height and weight were undertaken. Upon weight stabilisation, the plants' dry yield was gauged.

3. Results

3.1. Mineralogical and Morphological Characterisations of Nanocomposites

On XRD patterns, the added ADP is characterised by major reflections at 8.9, 7.1, and 3.8 Å (Figure 2). The intensity of these ADP peaks for GkNa90P10 is slightly higher than for other nanocomposites. The mineral composition in the nanocomposites is represented by the glauconite with quartz. The XRD pattern of glauconite shows reflections at 10.0, 4.5, and 2.6 Å . Reflections at 4.2, 3.4, 2.5, and 2.3 Å identify quartz. In addition, the XRD pattern of GkNa90P10 displayed reflections of the sodium carbonate at 6.4 and 2.9 Å (Figure 2). In glauconite, there is shift of the first basal reflection (001) in the direction of an increase in the interplanar distance up to 13.2–15.4 Å for nanocomposites produced via the chemical method, and up to 13.3–13.9 Å for nanocomposites produced via the mechanochemical process.

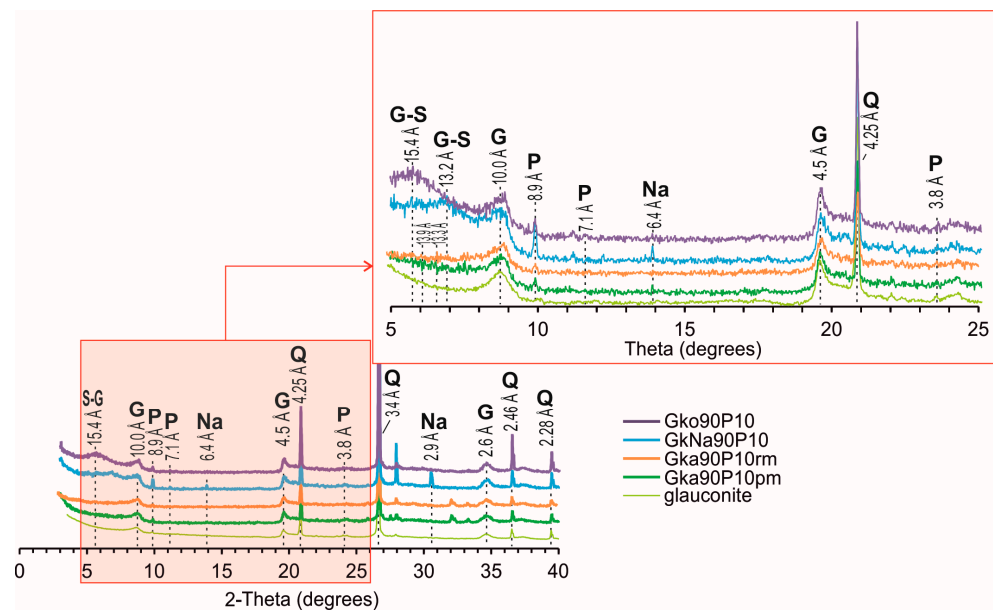


Figure 2. X-ray diffraction patterns of nanocomposites and glauconite fraction. G—glauconite; Na—sodium carbonate; P—ADP substances; Q—quartz.

The morphology of the chemically prepared Gko90P10 and GkNa90P10 nanocomposites retain their relic, globular, pellet glauconite grains with 100–400 μm in diameter and a characteristic internal structure (Figure 3A,B,E,F). Glauconite flakes are covered with a thin film of ADP of 0.4–2 μm thick. According to the EDS analysis, glauconite of Gko90P10 contains 5.3–8.1% potassium and 0.9–2.2% phosphorus of the covering thin film. The surface of the pellets is covered with ADP film with up to 6.9% of phosphorus (Figure 3H) and thickness up to 2–8 μm .

Microparticles represent the morphology of the mechanochemically produced Gka90P10rm and Gka90P10pm nanocomposites with sizes of 40–120 μm in diameter and a weakly preserved glauconite structure (Figure 3I,J,M,N). The structure of glauconite microparticles is represented by modified flakes less than 4 μm in size. The surface of the microparticles is covered with ADP films and aggregates (Figure 3). The microparticles are composed of phosphorus of 2.0–10.1%, potassium of 3.6–7.8%, and nitrogen of up to 2.3%.

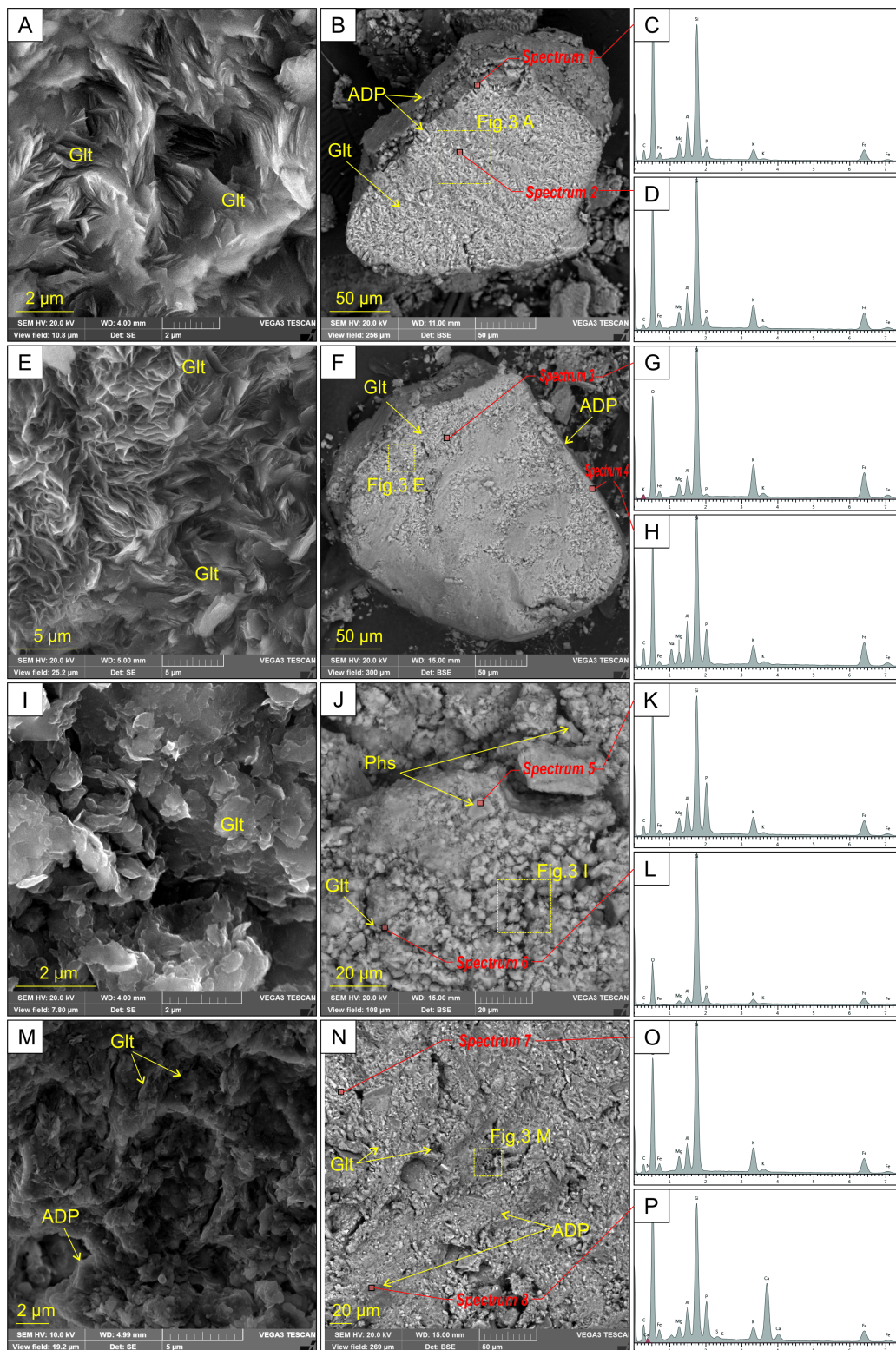


Figure 3. High-resolution SEM images, overview SEM images, and representative EDS spectra of nanocomposites: (A–D) Gko90P10; (E–H) GkNa90P10; (I–L) Gka90P10rm; (M–P) Gka90P10pm. SEM images show glauconite original flakes (A,E), glauconite deformed flakes (I,M), pellets (B,F) and microparticles (J,N) covered with a thin film with a high proportion of phosphorus (C,H,K,P) according to EDS analysis. The covering film of glauconite pellets contains up to 6.9% phosphorus (D,H). Glt—glauconite; ADP—ADP substances.

3.2. Crystal Structure Characteristics of Nanocomposites

Glauconite particles comprise nano-scale spindles of mica crystallites with a layered structure on high-resolution TEM images of the original mineral and activated nanocomposites (Figure 4). The glauconite unit structure consists of tetrahedral, octahedral, and tetrahedral sheets and an interlayer. The unit structure thickness of the original glauconite (Figure 4A) is 9.9–11.5 Å (average 10.8 Å), in which the interlayer thickness varies within a range of 1.9–3.0 Å (average 2.5 Å). The mineral particles of nanocomposites prepared via the chemical methods (Figure 4B) contain glauconite spindles and phosphate nanocrystals. The glauconite unit structure of Gko90P10 and GkNa90P10 obtained via TEM images ranges from 9.3 to 14.7 Å (average 11.9 Å), in which the interlayer thickness is 2.4–4.2 Å (average 3.2 Å). The unit structure of the Gka90P10rm (Figure 4C) and Gka90P10pm nanocomposites varies from 9.7 to 13.4 Å (average 11.2 Å) with a 1.9–3.6 Å (average 3.0 Å) micro-thickness of the interlayer.

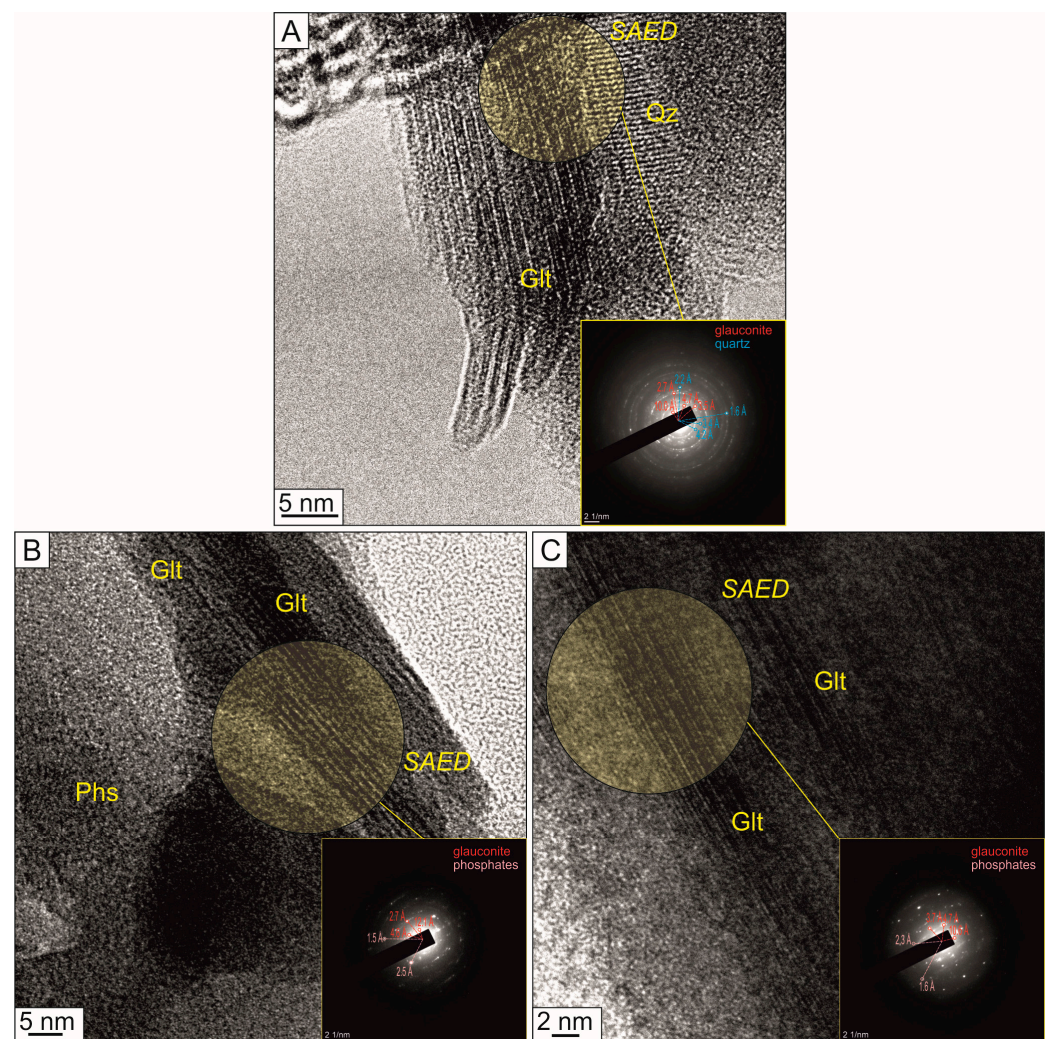


Figure 4. High-resolution TEM images of clay particles and SAED patterns with the main interpreted interplanar spaces of the original glauconite with impurities of quartz crystals (A), the produced Gko90P10 (B), and Gka90P10rm (C) nanocomposites. Glt—glauconite; Phs—phosphate crystals; Qz—quartz.

3.3. Chemical Characterisations of Nanocomposites

All FTIR spectra show vibrational bands related to the PO_4^{3-} phosphate ion (Figure 5); that is, bending vibrations at 546 cm^{-1} (O–P–O), gentle asymmetric vibrations at 906 cm^{-1} , 1097 cm^{-1} (P–O–H). The peaks at 796 and 799 cm^{-1} show Si–O stretching vibrations in the

tetrahedral sheet of the glauconite. A 1035 cm^{-1} peak characterises symmetric vibrations of Si–O of glauconite. Asymmetric deformation vibrations of N–H in NH_4^+ ions are reflected at 1280 cm^{-1} . Stretching vibrations of CH_2 are observed in the $2864\text{--}2914\text{ cm}^{-1}$. Asymmetric bending vibrations of OH^- ions in the octahedral positions of the mineral are reflected in the 3543 cm^{-1} bands. The CH_2 peaks at the range of $2864\text{--}2914\text{ cm}^{-1}$, as well as the PO_4^{3-} peak at the 1097 cm^{-1} and the NH_4^+ peak at the 1280 cm^{-1} , are more intense in GkNa90P10 and Gka90P10rm than in Gko90P10 and Gka90P10pm.

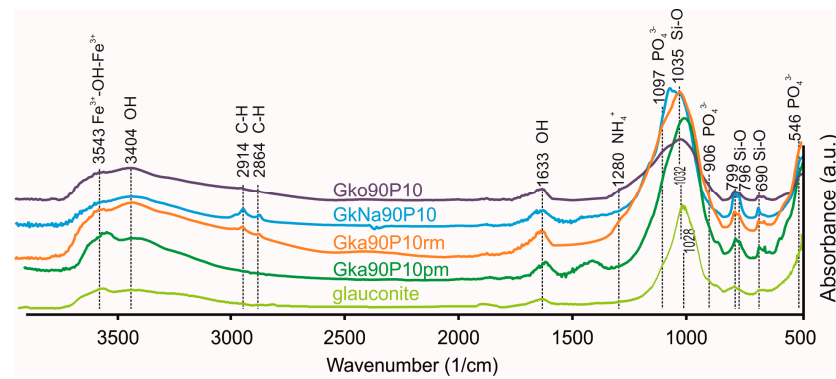


Figure 5. FTIR-spectra of nanocomposites and glauconite. The spectra of the nanocomposites differ in the presence of peaks for PO_4^{3-} , NH_4^+ , CH , and OH ions. All spectrums reflect Si–O and Fe^{3+} –OH vibrations of glauconite.

According to the TG analysis (Figure 6A, Table 1), six main stages of weight loss in the prepared nanocomposites are distinguished. Removal of free water by 0.9 wt.% occurs in the temperature range of $0\text{--}110\text{ }^\circ\text{C}$. In the range of $110\text{--}240\text{ }^\circ\text{C}$, weight losses are recorded at 1.1–3.2 wt.%, more than the original glauconite fraction. Perhaps these weight losses are associated with the release of adsorbed phosphates and water. Some ions, such as NH_3 , NH_2 , and H_2O , are observed in this temperature interval according to QMS analysis (Figure 6B). The maximum ion current intensity is typical for H_2O and NH_3 . A weight loss of 0.4–0.9 wt.% at the $240\text{--}302\text{ }^\circ\text{C}$ stage indicates the removal of adsorbed substances with a QMS peak of N_2O (Figure 6B). The weight losses in $302\text{--}365\text{ }^\circ\text{C}$ and $365\text{--}590\text{ }^\circ\text{C}$ vary in nanocomposites in the range of 2.5–3.3 wt.%, which are associated with the removal of interlayer solvating water from the mineral particles. The release of NO and N_2O is detected in this range (Figure 6B). An acute endothermic effect at $572\text{ }^\circ\text{C}$ corresponds to the quartz impurity. Weight loss in the range of $590\text{--}1000\text{ }^\circ\text{C}$ by 0.7–2.7 wt.% in nanocomposites indicates dehydroxylation of glauconite. The DSC curves of the nanocomposites show a gentle endothermic effect at $648\text{ }^\circ\text{C}$ in this interval. In the original glauconite, a weight loss of 0.6 wt.% is recorded in $590\text{--}1000\text{ }^\circ\text{C}$ without endothermic effect. In this temperature interval, a weak ion current intensity of N_2O and NO is noted (Figure 6B).

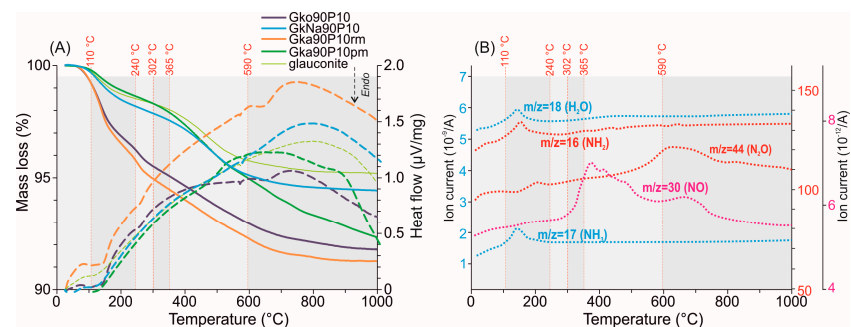


Figure 6. (A) TGA shown as continuous lines and DSC depicted with dotted lines for both nanocomposites and glauconite. (B) Chosen representative MS multi-ion detection curves ($m/z = 17$ (NH_3), 18 (H_2O), 30 (NO), and 44 (N_2O)) for Gko90P10 nanocomposite.

Table 1. Mass reduction data for glauconite–ADP nanocomposites in comparison with initial glauconite as per TGA.

	Nanocomposites	Weight Loss Intervals (°C)					
		0–110	110–240	240–302	302–365	365–590	590–1000
Weight loss (%)	Gko90P10	99.1	96.3	95.5	95.0	93.0	91.8
	GkNa90P10	99.6	98.2	97.9	97.4	95.2	94.4
	Gka90P10rm	99.1	95.9	94.9	94.4	92.3	91.3
	Gka90P10pm	99.8	98.7	98.3	97.8	95.0	92.3
	Glauconite	99.7	98.6	98.3	97.9	95.8	95.2
Final residue (%)	Gko90P10	0.9	2.8	0.8	0.5	1.9	1.2
	GkNa90P10	0.4	1.4	0.4	0.4	2.3	0.7
	Gka90P10rm	0.9	3.2	0.9	0.6	2.0	1.1
	Gka90P10pm	0.2	1.1	0.4	0.5	2.7	2.7
	Glauconite	0.3	1.1	0.3	0.4	2.1	0.6

3.4. Kinetic Nutrients Releases

The laboratory tests revealed varied leaching kinetics for ammonium, nitrate, potassium, and phosphate in the created glauconite–ADP nanocomposites. Observing ammonium (Figure 7A), two peak releases periods were identified: days 1st–7th and 21st–28th. Between days 7 and 21, ammonium is released slowly. Moreover, after day 28, ammonium has prolonged mobilisation kinetics, except for the GkNa90P10 nanocomposite. Ammonium release from the GkNa90P10 nanocomposite increases linearly from day 21 to day 56. The best kinetics of ammonium release was observed for the nanocomposites prepared chemically. Nitrates showcased a notable release rate within the initial seven days across all nanocomposites (Figure 7B). This was followed by a minimal leaching rate of 0.2–0.3 mg from days 7 to 56. Maximum nitrate release was observed in the chemically activated nanocomposites. Considering potassium release (Figure 7C), it experienced three to four primary stages that deviated from the reference plot. In all nanocomposites, the first two stages are synchronously recorded. The initial stage, culminating on the 7th day, marked a rapid release rate. The subsequent phase recorded a subdued release from the 7th to the 21st day. After day 21 of the soil column leaching experiments, the kinetics in different nanocomposites have some differences: in the nanocomposites prepared via chemical methods, the potassium dynamics are described by a consistent linear increase from day 21 to day 56; mechanochemically activated nanocomposites (Gk90P10rm and Gk90P10pm) release potassium in two steps during this period. The period from day 21 to day 43 showcased peak kinetics, while after the 43rd day, the release rate stabilised. The phosphate dynamics are maximal in the first 14 days of leaching, after which it has a prolonged character with low release levels (Figure 7D).

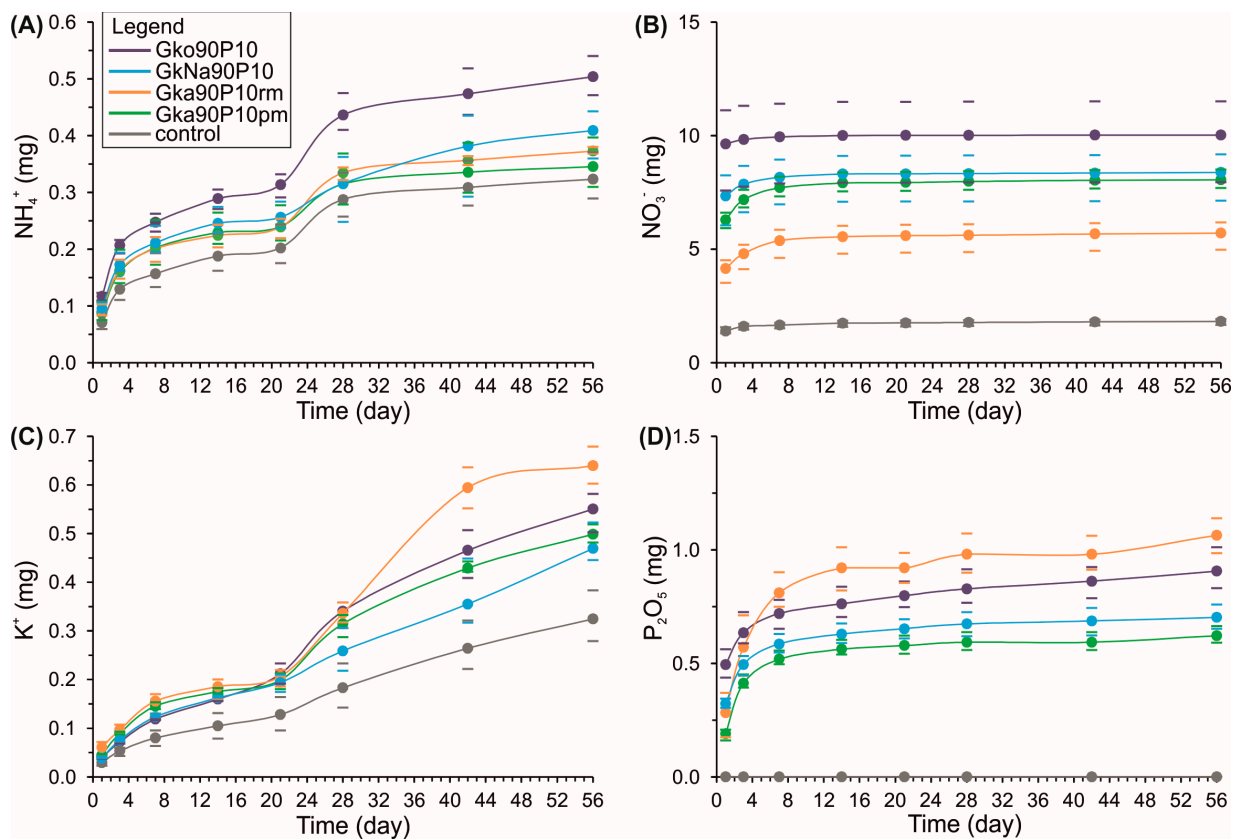


Figure 7. Cumulative curves of ammonium (A), nitrate (B), potassium (C), and phosphate (D) releases from nanocomposites glauconite–ADP, contrasted with a reference plot devoid of nanocomposites from lab experiments. Dashes show minimum and maximum cumulative values. The statistical significance of every parameter corresponds to the $p = 0.05$ level. Bars represent minimal and maximal values.

3.5. Influence of Nanocomposite on Plant Growth

The dry oat yield (*Avéna satíva*) increased in all variants of the experiments with the tested nanocomposites relative to the control (Figure 8). The dry weight (yield) changed in a range of 0.227–0.230 g for all plots, corresponding to 0.217 g for the control sample (Figure 8A). The yield in the plot with applied nanocomposites from glauconite–ADP mixtures increased by more than 4.6%. The germination rate (Figure 8B) when using nanocomposites varies in the range of 93.3–98.7%, while in the control plot (without fertilisers), this indicator is 93.0%. The maximum germination energy was noted for nanocomposites prepared mechanochemically in a planetary mill. The average plant height (Figure 8C) in the experiments with nanocomposites varied from 12.4 to 13.0 cm compared to 11.9 cm for the control sample. This corresponds to an increase in plant height of 4.6–9.9% when using nanocomposites.

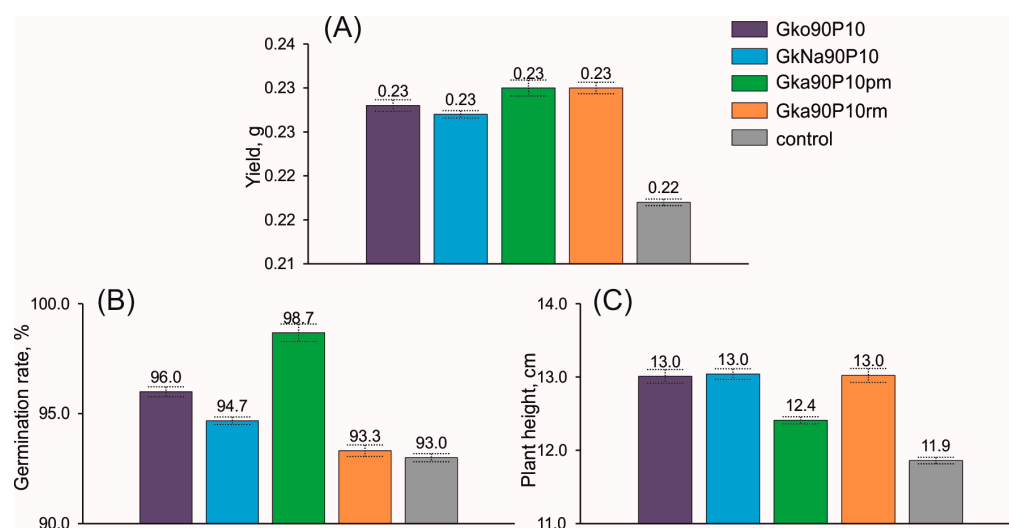


Figure 8. Dry yield (A), germination rate (B), and plant height (C) of oat (*Avena sativa*) due to application studied glauconite-ADP nanocomposite fertilisers based on the laboratory experiment. The statistical significance of every parameter indicates at the $p = 0.05$ level. Bars represent standard deviations.

4. Discussion

4.1. Characteristics of Glauconite-ADP Nanocomposites

The short shift in the slight basal reflection (001) in the bulk samples of nanocomposites (Figure 2) indicates that a significant part of the ADP was adsorbed on the basal interlayer planes of the mineral particles. This is confirmed by increased phosphorus content in the mineral aggregates (Figure 3C,D,G,H). In the Gka90P10rm and Gka90P10pm nanocomposites, the covering thin film on glauconite flakes contains up to 10.1% of the phosphorus (Figure 3K), which displays a slightly higher intensity of ADP peaks in the XRD pattern (Figure 2) and the FTIR spectrum (Figure 5) as the result of an increased adsorbed ADP relative to the Gko90P10 nanocomposite (Figure 3D). The preservation of the globular shape of the glauconite in the Gko90P10 and GkNa90P10 nanocomposites (Figure 2) is an advantage for their use as mineral fertiliser. The granular form improves the mechanical-physical properties of the soil and also allows for efficient fertilisation [7].

The unit structure thickness of some glauconite particles before and after chemical activation, according to the TEM data with SAED, varies from 9.9–11.5 Å to 9.3–14.7 Å (Figure 4), which indicates a slight expansion of the mineral crystal lattice, probably due to weak intercalation of ammonium into the interlayer of the mineral unit structure [41]. This is also reflected in the increase in the interlayer thickness from 1.9–3.0 Å to 2.4–4.2 Å. An insignificant part of NH_4^+ from ADP was most likely intercalated into the expanding structures of smectite layers in glauconite [75].

Deformation vibrations of phosphate ions are manifested in the FTIR spectra of nanocomposites (Figure 5) prepared via both chemical and mechanochemical techniques. Gentle asymmetric P–O–H oscillations at 906 cm^{-1} and 1097 cm^{-1} [80,81] are associated with the adsorbed part of the ADP on the mineral particles, including the edges of crystal basal surfaces. The intensity of these oscillations depends on the amount of ADP, which is connected with glauconite particles. The symmetric deformation vibrations of NH_4^+ indicate the intercalation of ammonium into the vacant space of the glauconite or smectite interlayer. Adsorbed ADP substances and intercalated ammonium will be released with a prolonged effect [25–27].

The total weight loss of the nanocomposites (Figure 6, Table 1) is 8.2 wt.%, 5.6 wt.%, 8.7 wt.%, and 7.7 wt.% for Gko90P10, GkNa90P10, Gka90P10rm, and Gka90P10pm, respectively, which is almost comparable to the initial added amount of ADP. The maximum adsorbed ADP varies from 2.8 to 3.2 wt.% for the Gko90P10 and Gka90P10rm nanocom-

posites, respectively, which is associated with the decomposition of a thin coating on the surface of mineral particles (Figure 3B,F). Adsorbed ADP into the micropore space is estimated at 0.4–0.9 wt.%, including the removal NH_3 , NH_2 , and H_2O ions. Substances (NO and N_2O) removal from the mineral interlayer space at 302–590 °C, a sharp endothermic effect at 572 °C, are synchronous for both the nanocomposites and the original glauconite. A gentle endothermic effect at 648 °C and the increased weight loss in nanocomposites relative to the original glauconite (Figure 6, Table 1) at 590–1000 °C prove the release of ADP from the mineral structure [82]. This is probably due to the incorporation of positively charged NH_4^+ ions on the edges of the octahedral basal planes of glauconite.

4.2. Advantages of Glauconite–ADP Nanocomposites

The prepared nanocomposites have similar features to previously studied complex composites consisting of monoammonium phosphate (or ADP) and kaolinite [83] or smectite [47,84]. However, glauconite, as an inhibitor of phosphates, is used for the first time, and it distinguishes the studied composites from composites with kaolinite or smectite as an inhibitor [41,59,83,85,86].

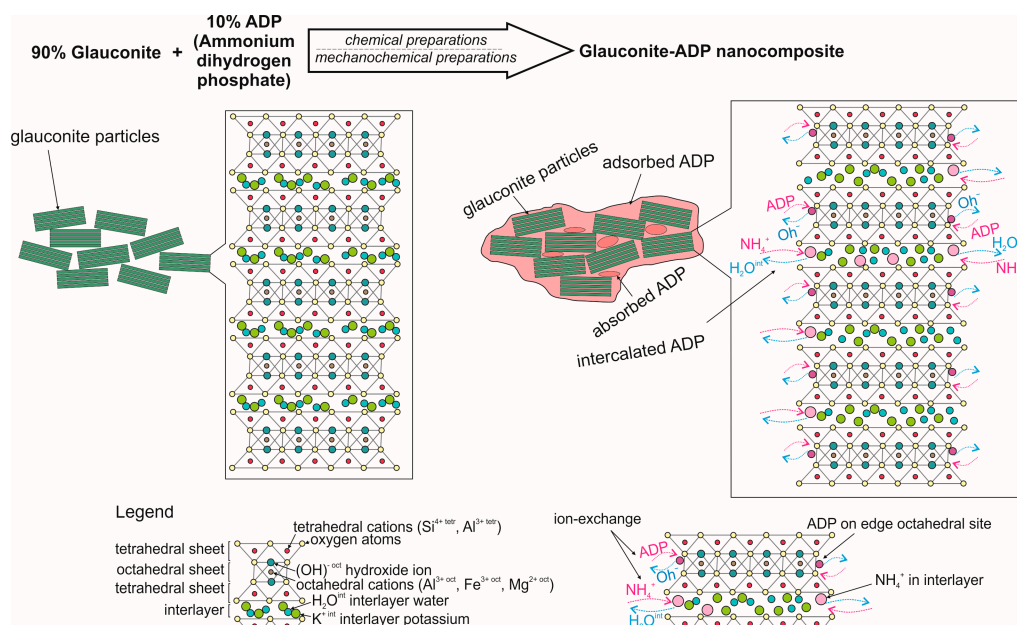
Nutrient discharges (such as ammonium, nitrate, potassium, and phosphates) present a sequential kinetic, linked to their association with the mineral, as depicted in Figure 7. The sequential patterns of nutrient release reflect their varied concentrations within the nanocomposites. It is postulated that easily accessible forms are tied to adsorbed substances in macro-pores dislodging from the nanocomposites primarily between days 1 to 21 or days 1 to 7, relevant to ammonium, nitrate, and phosphates, respectively. This is followed by a transition whereby adsorbed ammonium is liberated from the meso-pore space between the 21st and 28th days. The interlayered ammonium from the mineral interlayers is extracted by the 28th day of nanocomposite interaction with the soil. Generally, nanocomposites prepared via the mechanochemical method using glauconite–ADP combinations exhibit an added step. The sequential kinetics concerning nutrient leaches, particularly ammonium, potassium, and phosphates, endorse the dual advantageous role of stratified glauconite in nanocomposites, serving both as a deterrent for nutrients and as a potassium reservoir.

As a result of a series of laboratory experiments, it was found that the maximum stimulating effect on plant growth and development was exerted by nanocomposites prepared mechanochemically from mixtures of mineral and ADP in a 9:1 ratio (Figure 8). All plots with the investigated nanocomposite fertilisers demonstrated a stable positive effect on the growth and development of oats.

Glauconite–ADP nanocomposites prepared via chemical and mechanochemical methods have general advantages (Table 2). The interaction between glauconite and ADP at a ratio of 9:1 made it possible to create nanocomposites with four main types of ammonium phosphate nutrient: adsorbed in macro- and mesopore space; intercalated in the smectite interlayer; or adsorbed on the edge basal planes of mineral particles (Figure 9). Some essential portion of the NH_4^+ ions is intercalated into the interlayer space. The created nanocomposites, in addition to phosphates and ammonium, contain exchangeable potassium, which allows them to be evaluated as NPK fertilisers. Different forms of ADP in the nanocomposites and interlayer potassium will provide a controlled release of nutrients to plants. The chemical method allows for the preservation of the functional globular form of glauconite, while the two-stage mechanochemical method leads to a slight increase in the adsorption of ADP on the active surfaces of the mineral and intercalation of ammonium in interlayer of glauconite. The use of glauconite–ADP mixtures, for example, compared to glauconite–carbamide mixtures [75], has the benefit of creating complex NPK nanocomposite controlled-release fertilisers. Nanocomposite fertilisers derived from glauconite–ADP mixtures are particularly recommended for organic farming. This mineral, when used independently as an eco-friendly addition, enhances soil quality [72].

Table 2. Comparative features of glauconite–ADP nanocomposites.

Features	Nanocomposites			
	Gko90P10	GkNa90P10	Gka90P10rm	Gka90P10pm
A shift of the basal reflection 001 on the bulk XRD	Up to 15.4 Å	Up to 13.2 Å	Up to 13.3 Å	Up to 13.9 Å
Morphology of elementary particles	The relic globular and pellet grains with size of 100–400 μm		Microparticles with size of 40–120 μm	
ADP coating	2–8 μm thick film		Film and aggregates	
Mineral unit structure	The unit structure thickness is 9.3–14.7 Å (average: 11.9 Å)		The unit structure thickness is 9.7–13.4 Å (average: 11.2 Å)	
	The interlayer varies from 2.4 to 4.2 Å (average: 3.2 Å)		The interlayer varies from 1.9 to 3.6 Å (average: 3.0 Å)	
Adsorbed ADF in interparticle space (macropores)	2.8 wt.%	1.4 wt.%	3.2 wt.%	1.1 wt.%
Adsorbed ADF on edge plane (mesopores)	0.8 wt.%	0.4 wt.%	0.9 wt.%	0.4 wt.%
Intercalated NH ₄ ⁺	3.7 wt.%	3.4 wt.%	3.7 wt.%	6.0 wt.%

**Figure 9.** Schematic model of interactions between glauconite (90%) and ADP (10%) in the mechanochemical or chemical preparations of nanocomposites.

5. Conclusions

The study of the chemical and mechanochemical activation of glauconite–ADP nanocomposites at a ratio of 9:1 made it possible to draw the following conclusions.

The nanocomposites reflect a glauconite structure without significant expansion of the interplanar spaces of the mineral upon activation with ADP. The unit structure thickness of some elementary mineral particles increases due to the minimal intercalation of ammonium into the interlayer of glauconite.

The chemical method of preparing nanocomposites allows for obtaining substances in a preserved glauconite form. Globular and micro-aggregate particles in nanocomposites are

covered with a thin film of adsorbed ADP. The mechanochemical method slightly increases the proportion of adsorbed (up to 3.2 wt.%) and intercalated (up to 6.0 wt.%) ADP.

By using a potassium-containing clay mineral as an inhibitor, complex NPK nanocomposite fertilisers with controlled action were obtained. Targeted release of nutrients is expected due to various forms of nutrients on the surface, in the micropores, in the inter-layer space, and in the edge basal planes of glauconite. This is confirmed via the stepwise dynamics of the release of ammonium, nitrate, potassium, and phosphate from created nanocomposites.

Applying nanocomposites to soils as fertiliser stimulates an increase in yield, germination rate, and plant height.

Author Contributions: Conceptualization, M.R.; methodology, M.R., B.M. and A.L.-Q.; investigation, M.R., P.M., V.L., K.I., Y.G., A.K., B.M. and A.R.; resources, M.R. and A.R.; data curation, M.R., P.M., V.L., K.I., A.K., B.M. and Y.G.; writing—original draft preparation, M.R., B.M., A.L.-Q. and A.K.; visualization, M.R., P.M., K.I., Y.G., B.M. and A.R.; supervision, M.R. and A.L.-Q.; project administration, M.R., A.K. and A.R.; funding acquisition, M.R. All authors have read and agreed to the published version of the manuscript.

Funding: The authors gratefully acknowledge the financial support provided by Russian Science Foundation through the research project № 22-77-10002.

Data Availability Statement: Data is contained within the article.

Acknowledgments: A.R. acknowledges the project FSWW-2023-0010. The authors extend their gratitude to two anonymous reviewers and the editor for their objective criticism and valuable notes, which significantly contributed to the improvement of the manuscript.

Conflicts of Interest: The authors declare no conflict of interest.

References

1. Tilman, D.; Cassman, K.G.; Matson, P.A.; Naylor, R.; Polasky, S. Agricultural sustainability and intensive production practices. *Nature* **2002**, *418*, 671–677. [[CrossRef](#)] [[PubMed](#)]
2. Pretty, J.; Sutherland, W.J.; Ashby, J.; Auburn, J.; Baulcombe, D.; Bell, M.; Bentley, J.; Bickersteth, S.; Brown, K.; Burke, J.; et al. The top 100 questions of importance to the future of global agriculture. *Int. J. Agric. Sustain.* **2010**, *8*, 219–236. [[CrossRef](#)]
3. Tilman, D.; Fargione, J.; Wolff, B.; D’Antonio, C.; Dobson, A.; Howarth, R.; Schindler, D.; Schlesinger, W.H.; Simberloff, D.; Swackhamer, D. Forecasting agriculturally driven global environmental change. *Science* **2001**, *292*, 281–284. [[CrossRef](#)]
4. Fiorella, K.J.; Chen, R.L.; Milner, E.M.; Fernald, L.C.H. Agricultural interventions for improved nutrition: A review of livelihood and environmental dimensions. *Glob. Food Secur.* **2016**, *8*, 39–47. [[CrossRef](#)]
5. Trenkel, M.E. *Controlled-Release and Stabilized Fertilizers in Agriculture*; International Fertilizer Industry Association: Paris, France, 1997.
6. Matson, P.A. Agricultural Intensification and Ecosystem Properties. *Science* **1997**, *277*, 504–509. [[CrossRef](#)] [[PubMed](#)]
7. Liu, W.; Price, S.; Bennett, G.; Maxwell, T.M.R.; Zhao, C.; Walker, G.; Bunt, C. A landscape review of controlled release urea products: Patent objective, formulation and technology. *J. Control. Release* **2022**, *348*, 612–630. [[CrossRef](#)]
8. Akiyama, H.; Yan, X.; Yagi, K. Evaluation of effectiveness of enhanced-efficiency fertilizers as mitigation options for N₂O and NO emissions from agricultural soils: Meta-analysis. *Glob. Chang. Biol.* **2010**, *16*, 1837–1846. [[CrossRef](#)]
9. Xiao, Y.; Peng, F.; Zhang, Y.; Wang, J.; Zhuge, Y.; Zhang, S.; Gao, H. Effect of bag-controlled release fertilizer on nitrogen loss, greenhouse gas emissions, and nitrogen applied amount in peach production. *J. Clean. Prod.* **2019**, *234*, 258–274. [[CrossRef](#)]
10. Camargo, J.A.; Alonso, Á. Ecological and toxicological effects of inorganic nitrogen pollution in aquatic ecosystems: A global assessment. *Environ. Int.* **2006**, *32*, 831–849. [[CrossRef](#)]
11. Lasheen, E.S.R.; Zakaly, H.M.H.; Alotaibi, B.M.; Saadawi, D.A.; Ene, A.; Fathy, D.; Awad, H.A.; El Attar, R.M. Radiological Risk Parameters of the Phosphorite Deposits, Gebel Qulu El Sabaya: Natural Radioactivity and Geochemical Characteristics. *Minerals* **2022**, *12*, 1385. [[CrossRef](#)]
12. Wang, Z.; Chen, J.; Mao, S.; Han, Y.; Chen, F.; Zhang, L.; Li, Y.; Li, C. Comparison of greenhouse gas emissions of chemical fertilizer types in China’s crop production. *J. Clean. Prod.* **2017**, *141*, 1267–1274. [[CrossRef](#)]
13. Erisman, J.W.; Sutton, M.A.; Galloway, J.; Klimont, Z.; Winiwarer, W. How a century of ammonia synthesis changed the world. *Nat. Geosci.* **2008**, *1*, 636–639. [[CrossRef](#)]
14. Lu, C.; Tian, H. Global nitrogen and phosphorus fertilizer use for agriculture production in the past half century: Shifted hot spots and nutrient imbalance. *Earth Syst. Sci. Data* **2017**, *9*, 181–192. [[CrossRef](#)]
15. MacDonald, G.K.; Bennett, E.M.; Potter, P.A.; Ramankutty, N. Agronomic phosphorus imbalances across the world’s croplands. *Proc. Natl. Acad. Sci. USA* **2011**, *108*, 3086–3091. [[CrossRef](#)]

16. Cordell, D.; Drangert, J.O.; White, S. The story of phosphorus: Global food security and food for thought. *Glob. Environ. Chang.* **2009**, *19*, 292–305. [[CrossRef](#)]
17. Schachtman, D.P.; Reid, R.J.; Ayling, S.M. Phosphorus Uptake by Plants: From Soil to Cell. *Plant Physiol.* **1998**, *116*, 447–453. [[CrossRef](#)]
18. Shen, J.; Yuan, L.; Zhang, J.; Li, H.; Bai, Z.; Chen, X.; Zhang, W.; Zhang, F. Phosphorus dynamics: From soil to plant. *Plant Physiol.* **2011**, *156*, 997–1005. [[CrossRef](#)]
19. Moraes, P.I.R.; Tavares, S.R.; Vaiss, V.S.; Leitão, A.A. Investigation on sustainable phosphate release in agriculture: Structural and thermodynamic study of stability, dehydration and anionic exchange of Mg-Al-HPO₄ layered double hydroxide by DFT calculations. *Appl. Clay Sci.* **2018**, *162*, 428–434. [[CrossRef](#)]
20. Basak, B.B.B.; Gajbhiye, N.A.A. Phosphorus enriched organic fertilizer, an effective P source for improving yield and bioactive principle of Senna (*Cassia angustifolia* Vahl.). *Ind. Crops Prod.* **2018**, *115*, 208–213. [[CrossRef](#)]
21. Hermassi, M.; Valderrama, C.; Font, O.; Moreno, N.; Querol, X.; Batis, N.H.; Cortina, J.L. Phosphate recovery from aqueous solution by K-zeolite synthesized from fly ash for subsequent valorisation as slow release fertilizer. *Sci. Total Environ.* **2020**, *731*, 139002. [[CrossRef](#)]
22. Pogorzelski, D.; Filho, J.F.L.; Matias, P.C.; Santos, W.O.; Vergütz, L.; Melo, L.C.A. Biochar as composite of phosphate fertilizer: Characterization and agronomic effectiveness. *Sci. Total Environ.* **2020**, *743*, 140604. [[CrossRef](#)] [[PubMed](#)]
23. Wang, S.; Lv, X.; Fu, M.; Wang, Z.; Zhang, D.; Sun, Q. Risk assessment of Artemia egg shell-Mg-P composites as a slow-release phosphorus fertilizer during its formation and application in typical heavy metals contaminated environment. *J. Environ. Manag.* **2023**, *329*, 117092. [[CrossRef](#)] [[PubMed](#)]
24. Dou, Z.; Xie, X. Chitosan-Montmorillonite-Fe Nanocomposite Hydrogel for Phosphate Recovery and Reuse. *ACS ES T Eng.* **2022**, *3*, 682–689. [[CrossRef](#)]
25. Jariwala, H.; Santos, R.M.; Lauzon, J.D.; Dutta, A.; Wai Chiang, Y. Controlled release fertilizers (CRFs) for climate-smart agriculture practices: A comprehensive review on release mechanism, materials, methods of preparation, and effect on environmental parameters. *Environ. Sci. Pollut. Res.* **2022**, *29*, 53967–53995. [[CrossRef](#)] [[PubMed](#)]
26. Fu, J.; Wang, C.; Chen, X.; Huang, Z.; Chen, D. Classification research and types of slow controlled release fertilizers (SRFs) used—A review. *Commun. Soil Sci. Plant Anal.* **2018**, *49*, 2219–2230. [[CrossRef](#)]
27. Lawrencía, D.; Wong, S.K.; Low, D.Y.S.; Goh, B.H.; Goh, J.K.; Ruktanonchai, U.R.; Soottitantawat, A.; Lee, L.H.; Tang, S.Y. Controlled Release Fertilizers: A Review on Coating Materials and Mechanism of Release. *Plants* **2021**, *10*, 238. [[CrossRef](#)]
28. Rashid, M.; Hussain, Q.; Khan, K.S.; Alwabel, M.I.; Hayat, R.; Akmal, M.; Ijaz, S.S.; Alvi, S.; Rehman, O.U. Carbon-Based Slow-Release Fertilizers for Efficient Nutrient Management: Synthesis, Applications, and Future Research Needs. *J. Soil Sci. Plant Nutr.* **2021**, *21*, 1144–1169. [[CrossRef](#)]
29. Saraiva, R.; Ferreira, Q.; Rodrigues, G.C.; Oliveira, M. Phosphorous Nanofertilizers for Precise Application in Rice Cultivation as an Adaptation to Climate Change. *Climate* **2022**, *10*, 183. [[CrossRef](#)]
30. Wu, C.; Zhang, X.; Li, C.; Cheng, C.; Zheng, Y. Adsorption of Ammonium by Graphene Oxide-Based Composites Prepared by UV Irradiation and Using as Slow-Release Fertilizer. *J. Polym. Environ.* **2018**, *26*, 4311–4320. [[CrossRef](#)]
31. Oertli, J.J. Controlled-release fertilizers. *Fertil. Res.* **1980**, *1*, 103–123. [[CrossRef](#)]
32. Vejan, P.; Khadiran, T.; Abdullah, R.; Ahmad, N. Controlled release fertilizer: A review on developments, applications and potential in agriculture. *J. Control. Release* **2021**, *339*, 321–334. [[CrossRef](#)]
33. Zhang, H.; Liang, H.; Xing, L.; Ding, W.; Geng, Z.; Xu, C. Cellulose-based slow-release nitrogen fertilizers: Synthesis, properties, and effects on pakchoi growth. *Int. J. Biol. Macromol.* **2023**, *244*, 125413. [[CrossRef](#)] [[PubMed](#)]
34. Liu, J.; Yang, Y.; Gao, B.; Li, Y.C.; Xie, J. Bio-based elastic polyurethane for controlled-release urea fertilizer: Fabrication, properties, swelling and nitrogen release characteristics. *J. Clean. Prod.* **2019**, *209*, 528–537. [[CrossRef](#)]
35. Boyandin, A.N.; Kazantseva, E.A.; Varygina, D.E.; Volova, T.G. Constructing Slow-Release Formulations of Ammonium Nitrate Fertilizer Based on Degradable Poly(3-hydroxybutyrate). *J. Agric. Food Chem.* **2017**, *65*, 6745–6752. [[CrossRef](#)] [[PubMed](#)]
36. Atia, A.A.; Donia, A.M.; Hussin, R.A.; Rashad, R.T. Swelling and metal ion uptake characteristics of kaolinite containing poly [(acrylic acid)-co-acrylamide] hydrogels. *Desalination Water Treat.* **2009**, *3*, 73–82. [[CrossRef](#)]
37. Rashidzadeh, A.; Olad, A. Slow-released NPK fertilizer encapsulated by NaAlg-g-poly(AA-co-AAm)/MMT superabsorbent nanocomposite. *Carbohydr. Polym.* **2014**, *114*, 269–278. [[CrossRef](#)]
38. Wang, C.; Luo, D.; Zhang, X.; Huang, R.; Cao, Y.; Liu, G.; Zhang, Y.; Wang, H. Biochar-based slow-release of fertilizers for sustainable agriculture: A mini review. *Environ. Sci. Ecotechnol.* **2022**, *10*, 100167. [[CrossRef](#)]
39. Das, S.K.; Ghosh, G.K. Hydrogel-biochar composite for agricultural applications and controlled release fertilizer: A step towards pollution free environment. *Energy* **2022**, *242*, 122977. [[CrossRef](#)]
40. Abhíram, G.; Grafton, M.; Jeyakumar, P.; Bishop, P.; Davies, C.E.; McCurdy, M. Iron-rich sand promoted nitrate reduction in a study for testing of lignite based new slow-release fertilisers. *Sci. Total Environ.* **2023**, *864*, 160949. [[CrossRef](#)]
41. Borges, R.; Brunatto, S.F.; Leitão, A.A.; De Carvalho, G.S.G.; Wypych, F. Solid-state mechanochemical activation of clay minerals and soluble phosphate mixtures to obtain slow-release fertilizers. *Clay Miner.* **2015**, *50*, 153–162. [[CrossRef](#)]
42. Zhang, X.-M.; Hu, C.; He, Z.-Q.; Abbas, Y.; Li, Y.; Lv, L.-F.; Hao, X.-Y.; Gai, G.-S.; Huang, Z.-H.; Yang, Y.-F.; et al. Microcrystalline Apatite Minerals: Mechanochemical Activation for Agricultural Application. *Minerals* **2019**, *9*, 211. [[CrossRef](#)]

43. Rudmin, M.; Abdullayev, E.; Ruban, A.; Buyakov, A.; Soktoev, B. Mechanochemical Preparation of Slow Release Fertilizer Based on Glauconite–Urea Complexes. *Minerals* **2019**, *9*, 507. [[CrossRef](#)]
44. Pimsen, R.; Porrawatkul, P.; Nuengmacha, P.; Ramasoot, S.; Chanthai, S. Efficiency enhancement of slow release of fertilizer using nanozeolite–chitosan/sago starch-based biopolymer composite. *J. Coat. Technol. Res.* **2021**, *18*, 1321–1332. [[CrossRef](#)]
45. AlShamaileh, E.; Alrbaihat, M.; Moosa, I.; Abu-Afifeh, Q.; Al-Fayyad, H.; Hamadneh, I.; Al-Rawajfeh, A. Mechanochemical Preparation of a Novel Slow-Release Fertilizer Based on K_2SO_4 -kaolinite. *Agronomy* **2022**, *12*, 3016. [[CrossRef](#)]
46. Rudmin, M.; Banerjee, S.; Makarov, B.; Belousov, P.; Kurovsky, A.; Ibraeva, K.; Buyakov, A. Glauconite-Urea Nanocomposites As Polyfunctional Controlled-Release Fertilizers. *J. Soil Sci. Plant Nutr.* **2022**, *22*, 4035–4046. [[CrossRef](#)]
47. Chen, L.; Chen, X.L.; Zhou, C.H.; Yang, H.M.; Ji, S.F.; Tong, D.S.; Zhong, Z.K.; Yu, W.H.; Chu, M.Q. Environmental-friendly montmorillonite-biochar composites: Facile production and tunable adsorption-release of ammonium and phosphate. *J. Clean. Prod.* **2017**, *156*, 648–659. [[CrossRef](#)]
48. Maghsoodi, M.R.; Najafi, N.; Reyhanitabar, A.; Oustan, S. Hydroxyapatite nanorods, hydrochar, biochar, and zeolite for controlled-release urea fertilizers. *Geoderma* **2020**, *379*, 114644. [[CrossRef](#)]
49. Silva, I.A.; Silva, D.S.; Sousa, M.U.; Menezes, R.R.; Ferreira, H.S.; Neves, G.A. Encapsulation of nitrogen fertilizers in mixtures with organoclays for controlled release. *Clean Technol. Environ. Policy* **2020**, *1*, 3. [[CrossRef](#)]
50. McQuillan, R.V.; Stevens, G.W.; Mumford, K.A. Implementation of Biodegradable Liquid Marbles as a Novel Controlled Release Fertilizer. *ACS Sustain. Chem. Eng.* **2022**, *11*, 122–132. [[CrossRef](#)]
51. Souza, J.L.; de Campos, A.; França, D.; Faez, R. PHB and Montmorillonite Clay Composites as KNO_3 and NPK Support for a Controlled Release. *J. Polym. Environ.* **2019**, *27*, 2089–2097. [[CrossRef](#)]
52. Rudmin, M.; Banerjee, S.; Makarov, B.; Ibraeva, K.; Konstantinov, A. Mechanical Activation of Smectite-Based Nanocomposites for Creation of Smart Fertilizers. *Appl. Sci.* **2022**, *12*, 809. [[CrossRef](#)]
53. Rukchonlatee, S.; Siriphannon, P. Facile Preparation of Montmorillonite/Crosslinked Chitosan Containing Potassium Nitrate Nanocomposites as Eco-Friendly Slow Release Fertilizers. *J. Polym. Environ.* **2023**, *31*, 3454–3465. [[CrossRef](#)]
54. Slomp, C.P. Vivianite blues. *Nat. Geosci.* **2023**, *16*, 394. [[CrossRef](#)]
55. Fatimah, I.; Yudha, S.P.; Rubiyanto, D.; Widodo, I.D. Methenamine-smectite clay as slow release fertiliser: Physicochemical and kinetics study. *Chem. Eng. Trans.* **2017**, *56*, 1639–1644. [[CrossRef](#)]
56. Borges, R.; Baika, L.M.; Grassi, M.T.; Wypych, F. Mechanochemical conversion of chrysotile/ K_2HPO_4 mixtures into potential sustainable and environmentally friendly slow-release fertilizers. *J. Environ. Manag.* **2018**, *206*, 962–970. [[CrossRef](#)] [[PubMed](#)]
57. Rudmin, M.; Banerjee, S.; Yakich, T.; Tabakaev, R.; Ibraeva, K.; Buyakov, A.; Soktoev, B.; Ruban, A. Formulation of a slow-release fertilizer by mechanical activation of smectite/glauconite and urea mixtures. *Appl. Clay Sci.* **2020**, *196*, 105775. [[CrossRef](#)]
58. Makó, É.; Kristóf, J.; Horváth, E.; Vágvölgyi, V. Kaolinite-urea complexes obtained by mechanochemical and aqueous suspension techniques—A comparative study. *J. Colloid Interface Sci.* **2009**, *330*, 367–373. [[CrossRef](#)]
59. Al-Rawajfeh, A.E.; AlShamaileh, E.M.; Alrbaihat, M.R. Clean and efficient synthesis using mechanochemistry: Preparation of kaolinite- KH_2PO_4 and kaolinite- $(NH_4)_2HPO_4$ complexes as slow released fertilizer. *J. Ind. Eng. Chem.* **2019**, *73*, 336–343. [[CrossRef](#)]
60. Ni, B.; Liu, M.; Lü, S.; Xie, L.; Wang, Y. Environmentally Friendly Slow-Release Nitrogen Fertilizer. *J. Agric. Food Chem.* **2011**, *59*, 10169–10175. [[CrossRef](#)]
61. Lei, Z.; Cagnetta, G.; Li, X.; Qu, J.; Li, Z.; Zhang, Q.; Huang, J. Enhanced adsorption of potassium nitrate with potassium cation on H_3PO_4 modified kaolinite and nitrate anion into Mg-Al layered double hydroxide. *Appl. Clay Sci.* **2018**, *154*, 10–16. [[CrossRef](#)]
62. Rutkai, G.; Makó, É.; Kristóf, T. Simulation and experimental study of intercalation of urea in kaolinite. *J. Colloid Interface Sci.* **2009**, *334*, 65–69. [[CrossRef](#)] [[PubMed](#)]
63. Alshameri, A.; He, H.; Zhu, J.; Xi, Y.; Zhu, R.; Ma, L.; Tao, Q. Adsorption of ammonium by different natural clay minerals: Characterization, kinetics and adsorption isotherms. *Appl. Clay Sci.* **2018**, *159*, 83–93. [[CrossRef](#)]
64. Abukhadra, M.R.; Ali, S.M.; Nasr, E.A.; Mahmoud, H.A.A.; Awwad, E.M. Effective Sequestration of Phosphate and Ammonium Ions by the Bentonite/Zeolite Na-P Composite as a Simple Technique to Control the Eutrophication Phenomenon: Realistic Studies. *ACS Omega* **2020**, *5*, 14656–14668. [[CrossRef](#)]
65. Manna, S.; Das, P.; Basak, P.; Sharma, A.K.; Singh, V.K.; Patel, R.K.; Pandey, J.K.; Ashokkumar, V.; Pugazhendhi, A. Separation of pollutants from aqueous solution using nanoclay and its nanocomposites: A review. *Chemosphere* **2021**, *280*, 130961. [[CrossRef](#)] [[PubMed](#)]
66. Odin, G.S.; Matter, A. De glauconiarum origine. *Sedimentology* **1981**, *28*, 611–641. [[CrossRef](#)]
67. Guggenheim, S.; Adams, J.M.; Bain, D.C.; Bergaya, F.; Brigatti, M.F.; Drits, V.A.; Formoso, M.L.L.; Galan, E.; Kogure, T.; Stanjek, H. Summary of recommendations of nomenclature committees relevant to clay mineralogy: Report of the Association International pour l'Etude des Argiles (AIPEA) Nomenclature Committee for 2006 (Clays and Clay Minerals). *Clays Clay Miner.* **2007**, *55*, 761–772. [[CrossRef](#)]
68. Rudmin, M.; Banerjee, S.; Mazurov, A.; Makarov, B.; Martemyanov, D. Economic potential of glauconitic rocks in Bakchar deposit (S-E Western Siberia) for alternate potash fertilizer. *Appl. Clay Sci.* **2017**, *150*, 225–233. [[CrossRef](#)]
69. Rudmin, M.; Banerjee, S.; Makarov, B.; Mazurov, A.; Ruban, A.; Oskina, Y.; Tolkachev, O.; Buyakov, A.; Shaldybin, M. An investigation of plant growth by the addition of glauconitic fertilizer. *Appl. Clay Sci.* **2019**, *180*, 105178. [[CrossRef](#)]

70. Karimi, E.; Abdolzadeh, A.; Sadeghipour, H.R.; Aminei, A. The potential of glauconitic sandstone as a potassium fertilizer for olive plants. *Arch. Agron. Soil Sci.* **2012**, *58*, 983–993. [[CrossRef](#)]
71. Castro, L.; Tourn, S. Direct Application of Phosphate Rocks and Glauconite as Alternative Sources of Fertilizer in Argentina. *Explor. Min. Geol.* **2003**, *12*, 71–78. [[CrossRef](#)]
72. Rudmin, M.; Banerjee, S.; Makarov, B. Evaluation of the Effects of the Application of Glauconitic Fertilizer on Oat Development: A Two-Year Field-Based Investigation. *Agronomy* **2020**, *10*, 872. [[CrossRef](#)]
73. Franzosi, C.; Castro, L.N.; Celeda, A.M. Technical Evaluation of Glauconites as Alternative Potassium Fertilizer from the Salamanca Formation, Patagonia, Southwest Argentina. *Nat. Resour. Res.* **2014**, *23*, 311–320. [[CrossRef](#)]
74. McRae, S.G. Glauconite. *Earth-Sci. Rev.* **1972**, *8*, 397–440. [[CrossRef](#)]
75. Rudmin, M.; Maximov, P.; Dasi, E.; Kurovsky, A.; Gummer, Y.; Ibraeva, K.; Kutugin, V.; Soktoev, B.; Ponomarev, K.; Tararushkin, E.; et al. Intercalation of carbamide to globular glauconite by chemical processing for the creation of slow-release nanocomposites. *Appl. Clay Sci.* **2023**, *243*, 107075. [[CrossRef](#)]
76. Moore, D.M.; Reynolds, R.C., Jr. *X-ray Diffraction and the Identification and Analysis of Clay Minerals*; Oxford University Press: Oxford, UK, 1997.
77. Hillier, S. Quantitative Analysis of Clay and other Minerals in Sandstones by X-ray Powder Diffraction (XRPD). In *Clay Mineral Cements in Sandstones*; Blackwell Publishing Ltd.: Oxford, UK, 2003; pp. 213–251. ISBN 9781444304336.
78. Bish, D.L.; Post, J.E. Quantitative mineralogical analysis using the Rietveld full-pattern fitting method. *Am. Mineral.* **1993**, *78*, 932–940.
79. Taylor, J.C. Computer Programs for Standardless Quantitative Analysis of Minerals Using the Full Powder Diffraction Profile. *Powder Diffr.* **1991**, *6*, 2–9. [[CrossRef](#)]
80. Khan, A.Z.; Khan, Z.S.; Patle, S.; Rewatkar, K.G.; Zodape, S. FTIR spectral analysis of glycine doped ammonium dihydrogen phosphate (ADP) crystal. *J. Phys. Conf. Ser.* **2021**, *1913*, 012028. [[CrossRef](#)]
81. Yang, S.S.; Chen, Z.B. The Study on Aging and Degradation Mechanism of Ammonium Polyphosphate in Artificial Accelerated Aging. *Procedia Eng.* **2018**, *211*, 906–910. [[CrossRef](#)]
82. Emmerich, K.; Madsen, F.T.; Kahr, G. Dehydroxylation behavior of heat-treated and steam-treated homoionic cis-vacant montmorillonites. *Clays Clay Miner.* **1999**, *47*, 591–604. [[CrossRef](#)]
83. Alrbaihat, M.R.; Al-Rawajfeh, A.E.; Alshamaileh, E. A mechanochemical preparation, properties and kinetic study of kaolin-N, P fertilizers for agricultural applications. *J. Mech. Behav. Mater.* **2021**, *30*, 265–271. [[CrossRef](#)]
84. Mortland, M.M.; Fripiat, J.J.; Chaussidon, J.; Uytterhoeven, J. Interaction between ammonia and the expanding lattices of montmorillonite and vermiculite. *J. Phys. Chem.* **1963**, *67*, 248–258. [[CrossRef](#)]
85. Solihin; Zhang, Q.; Tongamp, W.; Saito, F. Mechanochemical synthesis of kaolin-KH₂PO₄ and kaolin-NH₄H₂PO₄ complexes for application as slow release fertilizer. *Powder Technol.* **2011**, *212*, 354–358. [[CrossRef](#)]
86. Sharma, N.; Singh, A.; Dutta, R.K. Biodegradable fertilizer nanocomposite hydrogel based on poly(vinyl alcohol)/kaolin/diammonium hydrogen phosphate (DAhP) for controlled release of phosphate. *Polym. Bull.* **2021**, *78*, 2933–2950. [[CrossRef](#)]

Disclaimer/Publisher's Note: The statements, opinions and data contained in all publications are solely those of the individual author(s) and contributor(s) and not of MDPI and/or the editor(s). MDPI and/or the editor(s) disclaim responsibility for any injury to people or property resulting from any ideas, methods, instructions or products referred to in the content.